ZAMM - JOURNAL OF APPLIED MATHEMATICS AND MECHANICS

https://onlinelibrary.wiley.com/journal/15214001

Impact factor:1.603

Accepted December 15th 2022

TRANSIENT SOLUTE DISPERSION IN ELECTRO-OSMOTIC VISCOPLASTIC FLOW IN A MICROCHANNEL

Ashis Kumar Roy[1] , Sudip Debnath[2,*] and O. Anwar Bég[3]

[1]*Department of Science and Humanities, Narsingarh, Tripura -799009,* ***India***

[2]*Professor and Director-Multi-Physical Engineering Sciences Group, Mechanical Engineering Department, School of Science, Engineering and Environment (SEE), University of Salford, Manchester,* ***UK***

Abstract: The transport of a neutral solute in incompressible electro-osmotic flow of Bingham plastic non-Newtonian liquid flowing through a microchannel is studied theoretically. The flow is driven by a constant axially applied electric field. The non-dimensional conservation equations with associated boundary conditions are solved with Gill's series expansion technique. The whole dispersion transport process is analyzed using three transport coefficients, viz., advection coefficient, dispersion coefficient and the apparent asymmetry coefficient, respectively. The mean concentration distribution of the solute is calculated via a third-order approximation of the series expansion. The study investigates the collective effects of yield stress and Electric Double Layer (EDL) thickness (inverse Debye length) on the transport of solute. The long-term behaviour of mean concentration distribution is shown to be accurately predicted by second-order approximations; however utilizing third or higher order approximations in Gill's series expansion enables a more refined analysis of the small and moderate time behavior of transport coefficients. The present analysis is relevant to emerging applications in bio-microfluidics exploiting electroviscous fluent media.

Keywords: *Electro-osmotics; non-Newtonian; Bingham liquid; hydrodynamic dispersion; Series expanions; advection coefficient; dispersion coefficient; apparent asymmetry coefficient; electrical double layer; microfluidics.*

1. Introduction

Taylor [1] dispersion is a micro-capillary flow-based technique in which a solute slug is injected into a solvent flowing in a laminar stream. The axial spreading of the solute is produced by the combined action of radial diffusion and convection. Taylor dispersion is a robust approach for determining

*Corresponding author - Sudip Debnath, Vellore Institute of Technology, Chennai Email: sudipdebnath49@gmail.com

molecular dispersion coefficients (and thus hydrodynamic radii). Over the years, the idea of Taylor dispersion has been explored by several authors (Aris [2], Gill [3], Chatwin [4], Gill and Sankarasubramanian [5], Barton [6], Mazumder and Das [7], Ng [8], Wu and Chen [9], Rana and Murthy [10], Wang and Chen [11], Roy et al. [12], Debnath et al. [13], etc.). These studies have continuously refined the original Taylor model to compute with increasing accuracy a variety of different transport coefficients. A knowledge of various transport coefficients is extremely useful in determining mixing process control in biomicrofluidics [14 - 16]. Taylor dispersion in microchannels also features in a variety of different engineering applications including microelectromechanical systems [17], drug delivery [18,19], component sensing, microscale mixing, etc. Lab-on-a-Chip technology is gaining a lot of attention because of its applications in the mixing and separation processes; consequently, diffusion and dispersion are desirable. Although there are numerous methods for achieving mixing, this task is difficult to perform in microscale conduits, so molecular diffusion, advection, and Taylor dispersion are used instead. Biochemical analysis needs effective mixing at the microscale. However, mixing in microchannels is often inhibited by laminar flow behavior since mixing is dominated by pure molecular diffusion. Molecular diffusion coefficient is however a material constant and cannot be improved. Nevertheless, different mixing mechanisms have been explored in the transport of a solute in microchannels which has emerged as a critical area of modern mirofluidics and has been explored by many authors both experimentally and theoretically. Interesting works include Smith et al. [20] on DNA macomolecular dispersion, Lagally et al. [21], on DNA amplification and Huiqian et al. [22] (on micromixer designs).

Increasingly modern microfluidics is deploying electro-kinetics which involves the interaction of electrical fields with aqueous ionic fluids. It features many intriguing effects including ion migration, electrical double layers, charged boundaries etc. In microchannel systems, electrical fields can be used to non-intrusively modify dispersion and improve mixing characteristics. Important applications of electroosmotic flow with Taylor dispersion include bacterial detection systems [23] and capillary electrophoresis analysis [24]. Several theoretical studies of hydrodynamic dispersion in electroosmotic transport have been communicated in recent years. These studies generally deploy Debye-Hückel linearization. Hoshyargar et al. [25] investigated both analytically and numerically the solute dispersion in electroosmotic flow through soft microchannels with low surface potential, presenting results for the solute concentration field and the effective dispersion coefficient. They showed that for thicker polyelectrolyte layers (PELs), a larger effective dispersion coefficient of a neutral solute band is produced. Dejam et al. [26] presented a mathematical model for advective-dispersive mass transfer in both purely pressure-driven (Poiseuille) flow, combined pressure-driven and electro-osmotic flow and also purely electro-osmotic flow (EOF) in a microfluidic channel. They deployed a reduced-order approach to extract the mass transfer coefficients, including the hydrodynamic dispersion and the effective advection coefficients, both of which were found to be functions of the Péclet number and the

velocity profile bluntness parameter. They further noted that there is a suppression in hydrodynamic dispersion for electro-osmotic flow compared with pressure-driven flow. Li and Jian [27] studied the unsteady solute dispersion in alternating current electroosmotic flow (AC EOF) through a slit polyelectrolyte-grafted (PE-grafted) nanochannel with interfacial slip using series expansion and Fourier transform methods. They showed that a critical value of oscillating Reynolds number exists below which the amplitude of dispersion coefficient increases whereas the mean concentration reduces (within the solute band). They also showed that amplitude of the dispersion coefficient is enhanced with increasing slip length and PEL thickness. Talebi et al. [28] computed electric potential and velocity distributions in hydrodynamic dispersion in fully developed electroosmotic flow throughsoft slit microchannels of dense polyelectrolyte layer (PEL). They observed that solute dispersion is amplified with increasing PEL-electrolyte permittivity difference whereas it is depleted with increasing PEL-electrolyte viscosity difference.

The above studies were confined to Newtonian fluids. However, in recent years, increasingly chemical and biomedical engineers have exploited non-Newtonian fluids [29] in micro-channel electroosmotics. The wide variety of rheological phenomena witnessed in such fluids including viscoplasticity, viscoelasticity, memory and shear-thinning/thickening enable modifications to be achieved in dispersion characteristics in micro-engineered systems. Interesting studies in this regard include Sharp [30] who considered Casson, power law and Bingham fluids and Dash et al. [31] (Casson model). Rana and Murthy [32] used asymptotic methods to determine three effective transport coefficients, i.e. exchange, convection and dispersion coefficients, in time-dependent solute dispersion in non-Newtonian flow in a tube with wall absorption. They deployed the Casson, Carreau and Carreau–Yasuda rheological models. They showed that for low shear rates, the Carreau fluid exhibits similar behaviour to a Newtonian fluid, whereas the Casson and Carreau–Yasuda model produces substantial modifications in the dispersion coefficients. Further investigations of non-Newtonian hydrodynamic dispersion include Rana and Murthy [33] (who used a two-phase Casson viscoplastic model), Debnath et al. [34, 35] (who deployed a three-layered model comprising a Casson fluid intercalated between two layers of Newtonian fluid), Roy and Bég [36] (micropolar and Newtonian fluids) and Roy et al. [37] (Casson fluids).

Dispersion in electro-osmotic flows of non-Newtonian fluids has also received some attention in recent years, again owing to emerging applications in biomicrofluidics. Arcos et al. [38] computed the dispersion coefficient of a passive solute in a steady-state pure electro-osmotic flow (EOF) of a viscoelastic fluid in a microchannel. They deployed the simplified Phan-Thien–Tanner (sPTT) model, and observed that viscoelasticity magnifies the axial distribution of the effective dispersion coefficients although there is a significant modification also with ratio of the half-height of the microchannel to the Debye length and electrical potential at the walls. Mukherjee et al. [39] also deployed a simplified

Phan–Thien Tanner (sPTT) model to study the solute dispersion in thermo-electro-osmotic rheological flows, with Joule heating and surface heat dissipation.

In the present study, a mathematical model is developed for transport of a neutral solute in incompressible electro-osmotic flow of a Bingham plastic non-Newtonian liquid flowing through a microchannel, under constant axially applied electric field. The non-dimensional conservation equations with associated boundary conditions are solved with Gill's series expansion technique. The dispsrsion transport coefficients, viz., advection coefficient, dispersion coefficient and the apparent asymmetry coefficient are computed with second order approximations and the mean concentration distribution of the solute is calculated via a third-order approximation of the series expansion. The effects of yield stress and Electric Double Layer (EDL) thickness (inverse Debye length) on the transport characteristics is scrutinized. The novelty of the present study is the simultaneous consideration of hydrodynamic dispersion and electro-osmotics for a Bingham viscoplastic liquid. The simulations are relevant to electrophoretic microengineered systems [40] including electrokinetic micromixers [41, 42]. To the authors' knowledge this is the first study to consider Taylor dispersion in bingham electro-osmotic transport and therefore extends previous non-Newtonian investigations which have considered, for example, power-law fluids [43] without hydrodynamic dispersion.

2. Mathematical formulation

As illustrated in **Fig.1**, the regime under investigation comprises the hydrodynamic dispersion in steady flow of non-Newtonian Bingham plastic electrolyte through a micro-channel bounded by two parallel plates separated by a distance, $2h$.

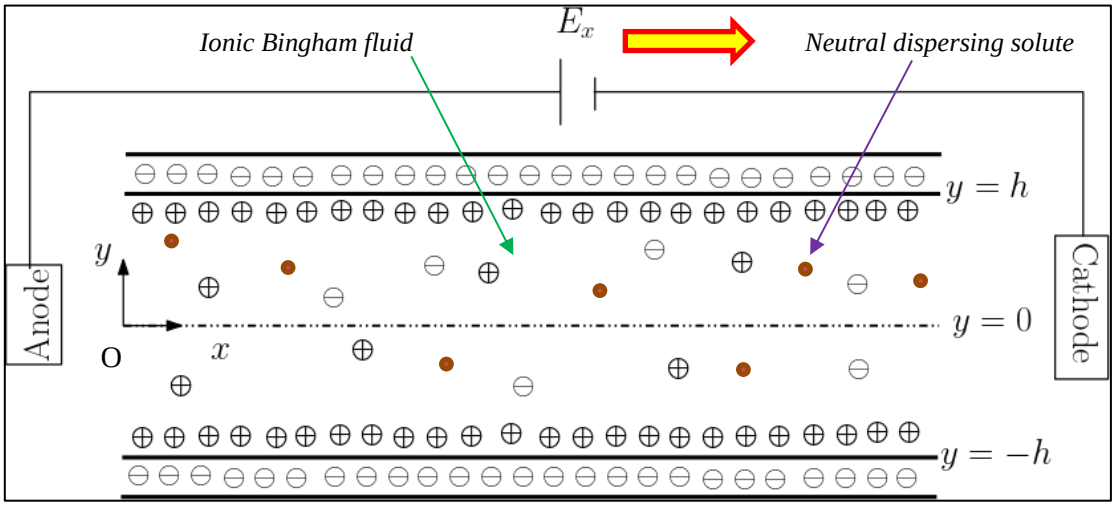

Figure 1: Schematic diagram of the proposed geometry

The flow geometry is defined in a Cartesian coordinate frame, with x directed along the plates (axial) and y directed normal to the plates (vertical). Both the walls are uniformly charged with a zeta potential

ζ and thus, when the solvent comes into touch with the channel walls, the Electric Double Layer (EDL) is formed. A constant electric (E_x) field is applied to drive the fluid flow in the x-direction. With all these assumptions in place, fluid flow is governed by following the momentum equation:

$$\frac{d\tau}{dy} + \rho_e E_x = 0 \tag{1}$$

Here, τ is shear stress and ρ_e is the charge density in the Electric Double Layer (EDL), which varies with channel height. The following Poison equation can be used to define the EDL (electrical) potential Ψ:

$$\frac{d^2\Psi}{dy^2} = -\frac{\rho_e}{\varepsilon}, \tag{2}$$

In Eq. (2) ε is the dielectric constant of the Bingham plastic liquid. Using Eqs. (1) and (2) and since $\tau = 0$ and $d\Psi/dy = 0$ at $y = 0$ (channel centreline) we can estimate shear stress distribution as:

$$\tau(y) = \varepsilon E_x \frac{d\Psi}{dy}, \tag{3}$$

The distribution of the electric potential is governed by the nonlinear Poisson–Boltzmann equation. Using the Debye–Hückel approximation [27], which assumes that electrolytes completely dissociate into ions in solution, that the solution is very dilute and that each ion is surrounded on average by ions of the opposite charge, however, the equation can be linearized, yielding,

$$\frac{d^2\Psi}{dy^2} = k^2\Psi, \tag{4}$$

Here k is characterized as the Debye-Hückel electro-osmotic parameter, the reciprocal of which is the Debye length of the EDL. A higher k value indicates a thinner double layer, while a lower k value indicates a thicker double layer. The condition that the EDL is much thinner than the channel height implies $k \gg 1$. As $\Psi = \zeta$ at the channel wall, i.e., at $y = \pm h$, the solution of Eq. (4) emerges as:

$$\Psi = \zeta \frac{\cosh(ky)}{\cosh(kh)}, \tag{5}$$

Using Eq. (5), the shear stress distribution (3) becomes:

$$\tau(y) = \varepsilon k \zeta E_x \frac{\sinh(ky)}{\cosh(kh)}, \tag{6}$$

In order to determine the velocity profile from the derived shear stress (6), we invoke the constitutive relation of the viscoplastic Bingham fluid model, which takes the form:

$$\begin{cases} \boldsymbol{\tau} = [\mu_0 + \tau_0/|\dot{\gamma}|]\,\dot{\boldsymbol{\gamma}} & \text{for } |\boldsymbol{\tau}| > \tau_0 \\ \dot{\boldsymbol{\gamma}} = 0 & \text{for } |\boldsymbol{\tau}| < \tau_0 \end{cases}, \tag{7}$$

Here $\boldsymbol{\tau}$ and $\dot{\boldsymbol{\gamma}}$ are, respectively, the shear stress and rate of deformation tensor and their magnitudes are given by $|\tau|$ and $|\dot{\gamma}|$. The other two rheological parameters μ_0 and τ_0 denote the plastic viscosity and yield stress of the flowing fluid. Yield stress is the threshold limit for triggered fluid motion, and accordingly, the flow profile is divided into *shear* and *unsheared* regions. Under simple shear, the constitutive Eq. (6) reduces to

$$\mu_0 \frac{du}{dy} = \begin{cases} \tau - \tau_0 & \text{for } |\tau| > \tau_0 \\ 0 & \text{for } |\tau| < \tau_0 \end{cases}, \tag{8}$$

To simplify our mathematical discussion, the following normalized variables are introduced:

$$\hat{y} = y/h, \quad \hat{k} = kh, \quad \hat{u} = u/(\tau_E/\mu_0 k), \quad (\hat{\tau}, \hat{\tau}_0) = (\tau, \tau_0)/\tau_E \tag{9}$$

here $\tau_E = -\varepsilon k \zeta E_x$, and $\tau_E/\mu_0 k = -\varepsilon \zeta E_x/\mu_0$ is the Smoluchowski slip velocity for a Newtonian fluid. With these normalized variables defined in Eq. (9), the appropriate stress distribution (6) and constitutive equation are:

$$\hat{\tau} = -\frac{\sinh(\hat{k}\,\hat{y})}{\cosh(\hat{k})}, \tag{10}$$

$$\frac{d\hat{u}}{d\hat{y}} = \begin{cases} \hat{k}(\hat{\tau} - \hat{\tau}_0) & \text{for } |\hat{\tau}| > \hat{\tau}_0 \\ 0 & \text{for } |\hat{\tau}| > \hat{\tau}_0 \end{cases} \tag{11}$$

The shear stress is maximum in magnitude at the channel walls, where it has the value $\tau_w = \tanh(\hat{k})$. In order to get non-uniform flow, $\tau_w > \tau_0$ and this leads to the formation of a yield surface in the flow regime. Denoting y_p is the location of the yield surface, then

$$y_p = \frac{1}{\hat{k}} \sinh^{-1}\left(\hat{\tau}_o \cosh\left(\hat{k}\right)\right), \text{for } \hat{\tau}_o < \tanh(\hat{k}) \tag{12}$$

Now, by solving Eq. (11) subject to no-slip boundary condition, i.e., $\hat{u} = 0$ at $\hat{y} = \pm 1$, and the velocity symmetry at the channel center i.e., $d\hat{u}/d\hat{y} = 0$ at $\hat{y} = 0$ we obtain the following velocity profile in the upper half of the channel ($0 \le \hat{y} \le 1$):

$$\hat{u} = \begin{cases} 1 - \dfrac{\cosh\left(\hat{k}\hat{y}\right)}{\cosh\left(\hat{k}\right)} - \hat{k}(1 - \hat{y}) \dfrac{\sinh(\hat{k}\hat{y}_p)}{\cosh(\hat{k})} & \text{for } \hat{y} > \hat{y}_p \\ 1 - \dfrac{\cosh(\hat{k}\hat{y}_p)}{\cosh(\hat{k})} - \hat{k}\,(1 - y_p) \dfrac{\sinh(\hat{k}\hat{y}_p)}{\cosh(\hat{k})} & \text{for } \hat{y} \le \hat{y}_p \end{cases} \tag{13}$$

Using the aforementioned velocity profile (13), Gill's dispersion analysis can then be conducted for mass transport, as described in the next section.

3. Mass transport

Let us consider the injection of a neutral solute in the electrolytic (ionic) Bingham fluid in the microchannel with a concentration of $C(t,x,y)$, and constant molecular diffusivity D. Then, the unsteady two-dimensional advection diffusion equation can be written as:

$$\frac{\partial C}{\partial t}+u\frac{\partial C}{\partial x}=D\left(\frac{\partial^2 C}{\partial x^2}+\frac{\partial^2 C}{\partial y^2}\right) \tag{14}$$

where, t represents the time.

Using the scaling parameters $\hat{C}=C/C_0$ and $\hat{t}=tD/h^2$ together with Eqn. (9) in Eq. (14), the *dimensionless* unsteady two-dimensional advection diffusion equation emerges as:

$$\frac{\partial \hat{C}}{\partial \hat{t}}+\mathrm{Pe}\,\hat{u}\frac{\partial \hat{C}}{\partial \hat{x}}=\left(\frac{\partial^2 \hat{C}}{\partial \hat{x}^2}+\frac{\partial^2 \hat{C}}{\partial \hat{y}^2}\right) \tag{15}$$

Here $\mathrm{Pe}=\tau_E h^2/\mu_0 kD$ denotes the Péclet number which quantifies the relative contribution of advection to diffusion in the dispersion process. In the subsequent analysis, the overhead carets are dropped for simplicity. Equation (15) is subject to following dimensionless boundary conditions:

$$C(x,y,t)=\delta(x)\ \text{at}\ t=0, \tag{16}$$

$$\frac{\partial C}{\partial y}=0\ \text{at}\ y=\pm 1, \tag{17}$$

$$C=0\ \text{at}\ x\to\pm\infty, \tag{18}$$

Gill generalized dispersion approach [3] is now invoked in order to estimate the effective dispersion coefficient:

$$C=C_{\mathrm{mean}}+\sum_{i=1}^{\infty}\chi_i\,(y,t)\frac{\partial^i C_{\mathrm{mean}}}{\partial x^i} \tag{19}$$

Here, $C_{\mathrm{mean}}=\frac{1}{2}\int_{-1}^{1}C\,(x,y,t)dy$ is the mean concentration of the neutral solute. Also, $\chi_i\,(y,t)$ ($i=1,2,3,\ldots\infty$) are functions of y and t to be determined.

Substituting Eq. (19) in Eq. (15), we obtain:

$$\begin{aligned}\frac{\partial C_{\mathrm{mean}}}{\partial t}+\mathrm{Pe}\,u\frac{\partial C_{\mathrm{mean}}}{\partial x}=\frac{\partial^2 C_{\mathrm{mean}}}{\partial x^2}-\sum_{i=1}^{\infty}\chi_i\frac{\partial^i}{\partial x^i}\left(\frac{\partial C_{\mathrm{mean}}}{\partial t}\right)-\sum_{i=1}^{\infty}\left(\frac{\partial \chi_i}{\partial t}-\frac{\partial^2 \chi_i}{\partial y^2}\right)\frac{\partial^i C_{\mathrm{mean}}}{\partial x^i}\\ -\mathrm{Pe}\,u\sum_{i=1}^{\infty}\chi_i\frac{\partial^{i+1}C_{\mathrm{mean}}}{\partial x^{i+1}}+\sum_{i=1}^{\infty}\chi_i\frac{\partial^{i+2}C_{\mathrm{mean}}}{\partial x^{i+2}}\end{aligned} \tag{20}$$

Again integrating Eq. (15) w.r.t y in the interval $[-1,1]$ we get:

$$\frac{\partial C_{\text{mean}}}{\partial t} = \frac{\partial^2 C_{\text{mean}}}{\partial x^2} - \frac{\text{Pe}}{2}\int_{-1}^{1} u\frac{\partial C}{\partial x}dy \tag{21}$$

Following Gill [3] we assume that the transverse average concentrations are diffusive in nature immediately from the time of solute injection, hence:

$$\frac{\partial C_{\text{mean}}}{\partial t} = K_1\frac{\partial C_{\text{mean}}}{\partial x} + K_2\frac{\partial^2 C_{\text{mean}}}{\partial x^2} + K_3\frac{\partial^3 C_{\text{mean}}}{\partial x^3} + \cdots \tag{22}$$

Using Eq. (19) in Eq. (21) and comparing with Eq. (22) we get:

$$K_i = \delta_{i2} - \frac{\text{Pe}}{2}\int_{-1}^{1} u\,\chi_{i-1}dy \tag{23}$$

$i = 1, 2, \cdots$ and $\chi_0 = 1$.

Equation (22) is an infinite series of derivatives of mean concentration also known as the *Taylor-Gill expansion equation*. Thus, the coefficients of every order of the derivatives represents several transport coefficients (Gill [3]). It is important to mention that the zeroth-order coefficient (K_0) vanishes as there is no chemical reaction present. Further, following the convective term in the advection-diffusion equation, one can consider K_1 as the advection coefficient. Thus, by virtue of K_1 we can discuss the transport mechanism when *convection dominates diffusion*. Similarly, the dispersion coefficient K_2, is the key parameter to study the mass transport considering *both axial and transverse diffusion* together with *convection*. In the present work, we have restricted the analysis up to third-order expansions in Eq. (22), and so K_3 is included. The purpose of K_3 is also significant while studying the nature of mass distribution. This coefficient, K_3 is termed the *apparent asymmetry coefficient*. It is worth noting that there are relatively few research articles (Jiang et al. [44], Jiang and Chen [45]) in which fourth-order approximations have been derived for the Taylor-Gill dispersion model. However considering the third-order dispersion model itself, only a very small change in the value of K_3, of approximately 10^{-5} is produced. Thus, to consider higher orders may not be required. From, Eq. (23), it is evident that the transport coefficients are coupled with the unknown function $\chi_i(y,t)$ ($i = 1, 2, 3, \ldots \infty$). In sections 4 and 5, the solutions of K_1, K_2 and K_3 are discussed in addition to the solutions of $\chi_1\,(y,t)$, $\chi_2\,(y,t)$ and $\chi_3\,(y,t)$, respectively.

4. Evaluation of advection (K_1) and dispersion (K_2) coefficients

From Eq. (23) for $i = 1$ we get:

$$-K_1/\text{Pe} = \left[1 - \frac{\tanh(k)}{k}\right] + \frac{\sinh(ky_p)}{\cosh(k)} \times \left[\frac{1}{k} + \frac{k}{2}\left(y_p^2 - 1\right)\right] - y_p\frac{\cosh(ky_p)}{\cosh(k)} \tag{24}$$

Thus, the advection coefficient $\boldsymbol{K_1}$ can be obtained from Eqn. (24), which is *independent of time* but is a function of yield stress and EDL thickness parameters.

To calculate the effective dispersion coefficient from Eq. (23), we must first determine $\chi_1(y,t)$, which can be done by solving the following differential equation (equating coefficient of $\partial C_{mean}/\partial x$ from Eq. (20) with the aid of Eq. (22)) with associated boundary conditions at the microchannel boundaries.

$$\frac{\partial \chi_1}{\partial t} = \frac{\partial^2 \chi_1}{\partial y^2} - \mathrm{Pe}(u - u_{\mathrm{mean}}) \tag{25}$$

$$\frac{\partial \chi_1}{\partial y} = 0 \text{ at } y = \pm 1 \tag{26}$$

$$\chi_1 = 0 \text{ at } t = 0 \tag{27}$$

Solving Eq. (25) subject to (26) and (27) we get:

$$\chi_1(y,t) = \sum_{n=0}^{\infty} \frac{2\mathrm{Pe}C_n}{n^2\pi^2}\cos(n\pi y)(\exp(-n^2\pi^2 t) - 1) \tag{28}$$

Where:

$$\begin{aligned} C_n = &\left[\frac{n\pi}{k^2 + n^2\pi^2} - \frac{1}{n\pi}\right]\frac{\cosh(ky_p)\sin(n\pi y_P)}{\cosh(k)} + \frac{(-1)^{n+1}k}{k^2 + n^2\pi^2}\tanh(k) \\ &+ \left[\frac{k}{k^2 + n^2\pi^2} - \frac{k}{n^2\pi^2}\right]\frac{\sinh(ky_p)\cos(n\pi y_p)}{\cosh(k)} + (-1)^n\frac{k}{n^2\pi^2}\frac{\sinh(ky_p)}{\cosh(k)} \end{aligned} \tag{29}$$

Using Eq. (28) in (23) for $i = 2$, one obtains the simplified form of the dispersion coefficient K_2 for the present model, as follows:

$$K_2(t) = 1 + 2\mathrm{Pe}^2\sum_{n=0}^{\infty}\frac{C_n^2}{n^2\pi^2}(1 - \exp(-n^2\pi^2 t)) \tag{30}$$

Equation (30) represents the unsteady effective dispersion coefficient for the Bingham plastic fluid with finite yield stress y_p. The special case of a Newtonian fluid is retrieved for $y_p \to 0$. Hence, the expression for the effective dispersion coefficient (K_2^N) for the case of a Newtonian fluid is given below:

$$K_2^{\mathrm{N}}(t) = \lim_{y_p \to 0} K_2(t) = 1 + 2\mathrm{Pe}^2\sum_{n=0}^{\infty}\frac{k^2\tanh^2(k)}{n^2\pi^2(k^2 + n^2\pi^2)^2}(1 - \exp(-n^2\pi^2 t)) \tag{31}$$

Eq. (31) is exactly matched with Paul and Ng. [46](see Eq. (59) in their article). Further, if $t \to \infty$, the effective dispersion coefficient is obtained for the steady state case, as:

$$K_{2,\mathrm{Steady}}^{\mathrm{N}} = \lim_{t \to \infty} K_2^{\mathrm{N}} = 1 + \mathrm{Pe}^2\left[\frac{5\tanh^2 k}{6k^2} - \frac{3\tanh k}{2k^3} + \frac{2\tanh^2 k}{k^4} - \frac{1}{2k^2}\right] \tag{32}$$

Eqn. (32) agrees with the result deduced by Griffiths and Nilson [47].

5. Evaluation of apparent asymmetry coefficient (K_3)

The transport coefficient $K_3(t)$ is related to the coefficient of skewness and is helpful to understand the nature of solute concentration distribution. Thus, one can name the transport coefficient as the *apparent asymmetry coefficient* (K_3). To evaluate K_3, here we have to determine χ_2 first from the equation in below (equating coefficient of $\partial^2 C_{mean}/\partial x^2$ from Eq. (20) with the aid of Eq. (22)) along with the boundary conditions:

$$\frac{\partial \chi_2}{\partial t} = \frac{\partial^2 \chi_2}{\partial y^2} - \mathrm{Pe}(u - u_{\mathrm{mean}})\chi_1 + (1 - K_2) \tag{33}$$

$$\frac{\partial \chi_2}{\partial y} = 0 \text{ at } y = \pm 1 \tag{34}$$

$$\chi_2 = 0 \text{ at } t = 0 \tag{35}$$

The solution of Eqn. (33) is:

$$\chi_2(y,t) = \frac{2\mathrm{Pe}^2}{\pi^4}\sum_{n=1}^{\infty}\sum_{k=1,m\neq n}^{\infty}\frac{C_m(C_{m+n}+C_{m-n})}{m^2}\cos(n\pi y)\times\left[\frac{\exp(-n^2\pi^2 t)-\exp(-m^2\pi^2 t)}{n^2-m^2} + \frac{1-\exp(-n^2\pi^2 t)}{n^2}\right] + \frac{2\mathrm{Pe}^2}{\pi^2}\sum_{n=1}^{\infty}\frac{C_n C_{2n}}{n^2}\cos(n\pi y)\times\left[\frac{1-\exp(-n^2\pi^2 t)}{n^2\pi^2} - t\exp(-n^2\pi^2 t)\right] \tag{36}$$

Hence, the solution for $K_3(t)$, is:

$$K_3(t) = -\frac{2\mathrm{Pe}^3}{\pi^4}\sum_{n=1}^{\infty}\sum_{k=1,m\neq n}^{\infty}\frac{C_m C_n(C_{m+n}+C_{m-n})}{m^2}\times\left[\frac{\exp(-n^2\pi^2 t)-\exp(-m^2\pi^2 t)}{n^2-m^2} + \frac{1-\exp(-n^2\pi^2 t)}{n^2}\right] + \frac{2\mathrm{Pe}^3}{\pi^2}\sum_{n=1}^{\infty}\frac{C_n^2 C_{2n}}{n^2}\times\left[t\exp(-n^2\pi^2 t) - \frac{1-\exp(-n^2\pi^2 t)}{n^2\pi^2}\right] \tag{37}$$

Taylor [1] (1953,1954a) has shown that at large time the *mean concentration* of the solute becomes a Gaussian function of distance along the tube axis and his experiments also largely confirm this fact. However, many experimental curves found by Taylor are not completely symmetric (Gaussian curves should be symmetric); one of the reasons behind this is that insufficient time has elapsed for asymmetries to become completely smoothed out. Aris [2] has shown theoretically that the *absolute skewness* of the mean concentration does tend to zero, but only as $1/\sqrt{t}$, where t is the time since injection. To capture this asymmetry at the initial stage the coefficient K_3 plays a vital rule. However, we have observed in our study that $K_3 \rightarrow 0$ for large times and indeed the mean concentration curve becomes Gaussian. In the results and discussion this issue has therefore been strongly highlighted.

6. Second and third order dispersion model

By truncating third terms onwards from Eq. (22) we obtain the *second order* approximation:

$$\frac{\partial C_{\text{mean}}^{(2)}}{\partial t} = K_1 \frac{\partial C_{\text{mean}}^{(2)}}{\partial x} + K_2(t) \frac{\partial^2 C_{\text{mean}}^{(2)}}{\partial x^2} \tag{38}$$

Here the superscript (2) indicates the approximation is due to the truncation from the third term onwards in the Gill dispersion model. This model is widely acceptable as it resembles the classical Taylor dispersion model. The solution of Eqn. (38) is:

$$C_{\text{mean}}^{(2)}(x,t) = \frac{1}{\sqrt{4\pi G_2(t)}} \exp\left\{-\frac{(x+K_1 t)^2}{4G_2(t)}\right\} \tag{39}$$

Here:

$$G_2(t) = \int_0^t K_2\,(t)dt \tag{40}$$

Clearly, the *second order mean concentration* (Eq.(39)) follows the *Gaussian distribution*. However, this is not the case at all times, particularly at the *initial stage* of solute distribution, for which the distribution is asymmetric [48,49,13]. Thus, to study the *asymmetry* in the solute concentration, a *third-order dispersion model* is proposed by truncating after the third term in Eq. (22), as follows:

$$\frac{\partial C_{\text{mean}}^{(3)}}{\partial t} = K_1 \frac{\partial C_{\text{mean}}^{(3)}}{\partial x} + K_2(t) \frac{\partial^2 C_{\text{mean}}^{(3)}}{\partial x^2} + K_3(t) \frac{\partial^3 C_{\text{mean}}^{(3)}}{\partial x^3} \tag{41}$$

As stated above, here the superscript (3) indicate the mean concentration is approximated by truncating from the fourth term onwards in the Gill dispersion model. The solution of Eqn. (40) is as:

$$C_{\text{mean}}^{(3)}(x,t) = \frac{1}{\sqrt[3]{-3G_3(t)}} \exp\left\{-\frac{G_2(t)}{3G_3(t)}x - \frac{K_1 G_2(t)}{3G_3(t)}t + \frac{2G_2^3(t)}{27G_3^2(t)}\right\} Ai\left[\frac{-x - K_1 t + \frac{G_2^2(t)}{3G_3(t)}}{\sqrt[3]{3G_3(t)}}\right] \tag{42}$$

where,

$$G_3(t) = \int_0^t K_3\,(t)dt \tag{43}$$

In the next section, the results for various model parameter values (yield stress, electro-osmotic etc) are presented in detail.

7. Results and Discussion

The study analytically investigates the transport of a neutral solute in the electro-osmotic flow of an electrolytic Bingham plastic fluid through a rectangular two-dimensional microchannel employing the transport coefficients viz., K_1, K_2 and K_3 obtained from Gill's series expansion. The transport process is assessed via the impact of the Debye-Hückel electro-osmotic parameter (k) or EDL thickness $(1/k)$ and with various yield stress (τ_0), respectively.

7.1 Axial velocity

Figure 2 shows the axial velocity distribution between the microchannel plates for different values of yield stress and Debye-Hückel parameter (EDL thickness). It can be seen from Fig. 2(a) that as the value of yield stress increases, the axial velocity in the core zone of the microchannel reduces i.e. axial flow deceleration in induced. In other words, the plug radius becomes an increasing function of yield stress in the parabolic flow profile for Bingham plastic fluid. The blunt plateau in the core zone is widened with greater yield stress.

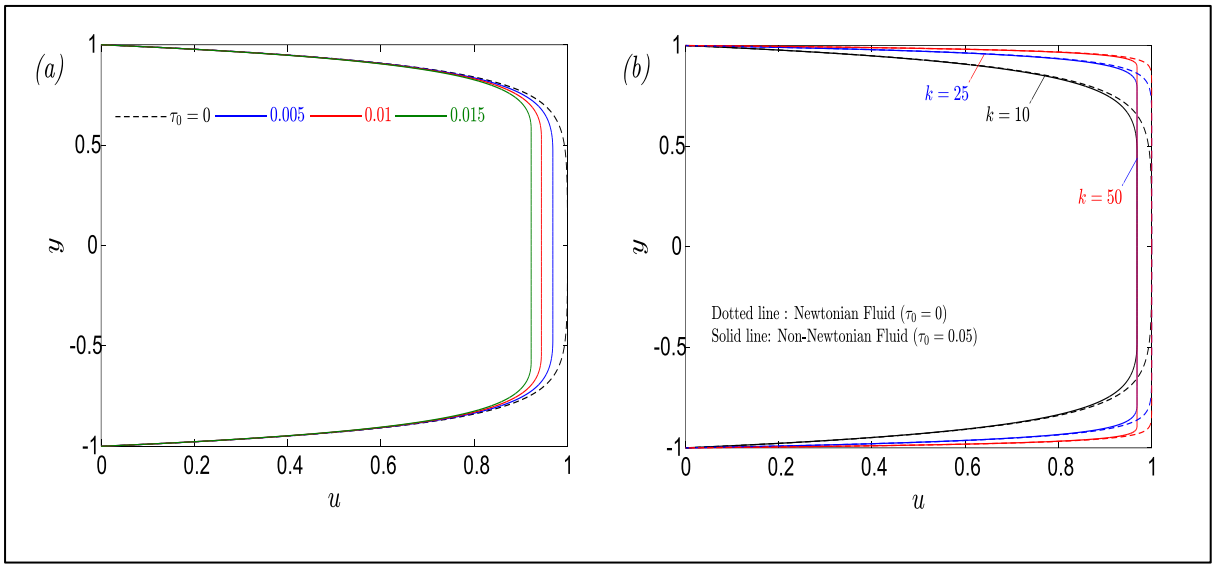

Figure 2: Axial velocity (u) variation with vertical coordinate (y) for (a) various yield stress values with $k = 10$, (b) various values of Debye-Hückel parameter.

Also, for the smaller values of k, the velocity profile is expected to remain parabolic (Fig. 2(b)), close to Poiseuille flow. However, as the value of k increases, the velocity profile in the core region becomes more uniform in the core region about the centreline, approaching a plug flow profile for large $k = 50$ and symmetry is maintained. The results are in good agreement with Paul and Ng [46] for the case of Newtonian fluid, i.e. vanishing yield stress, $\tau_0 = 0$ (Fig. 2(b)). This is attributable to the EDL at the solid surface exerting electrical forces on the ions in the liquid, which in turn restricts the motion of these ions. Therefore the presence of the EDL enhances the friction factor as well as the apparent

viscosity. The apparent viscosity may be several times higher than the bulk viscosity of the liquid [50], when the value of *k* is very small. Thus, a *lower* Debye-Hückel electro-osmotic parameter, i.e. a thicker electrical double layer (EDL), results in a larger portion of fluid being affected by the EDL. Consequently the fluid occupies a smaller volume within the channel flow region. In a similar way the distribution of fluid velocity for the larger *k* value can be explained.

7.2 Advection coefficient

The advection coefficient (K_1) is also extracted from Gill's series expansion to assess the role of advection velocity in the transport process. It can seen from Eq. (24) the advection coefficient is equivalent to the average flow velocity, which is not only deflected by the yield stress (τ_0), also affected by the Debye-Hückel parameter (k). In **Fig. 3**, the coupled effect of the parameters k and τ_0 on the advection coefficient function, -K_1/Pe is depicted. One can see, with the increase of time t the value of K_1 increases, whereas the magnitude of K_1 is reduced by the higher values of τ_0.

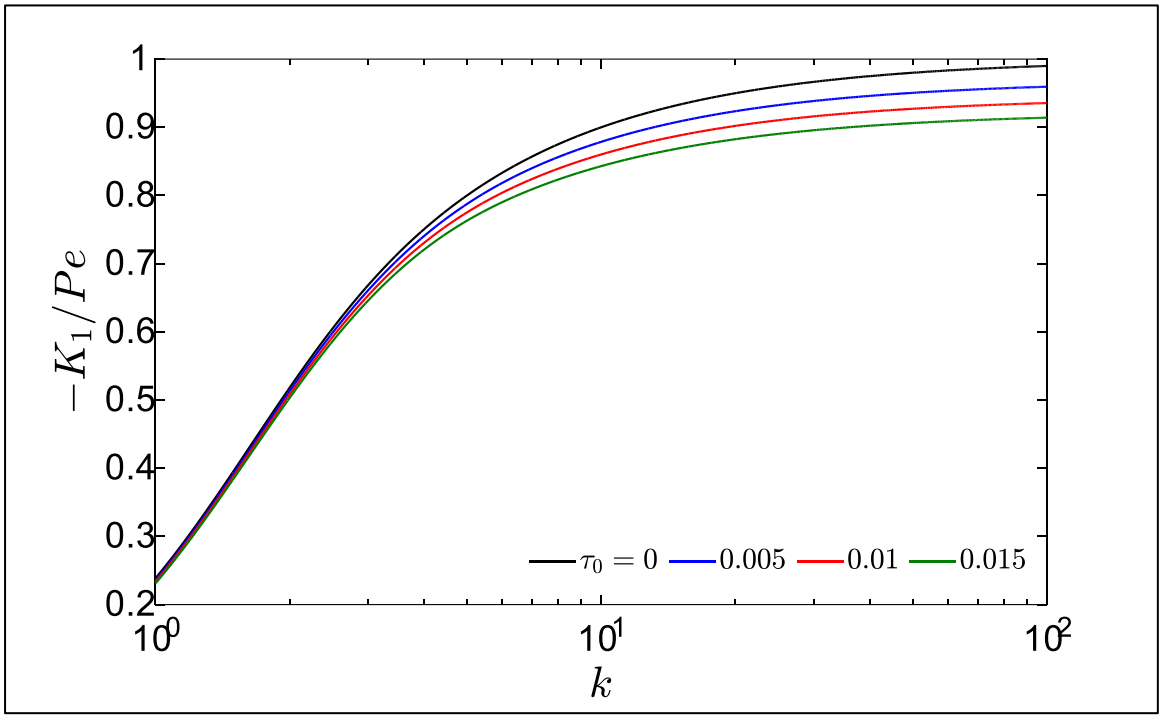

Figure 3: Advection coefficient/Péclet number with Debye-Hückel parameter for various yield stress.

The reduction of the advection coefficient function with higher values of yield stress is due to the deceleration in the flow with more strongly viscoplastic characteristics, since higher yield stress delays the inception of viscous flow, according to the nature of Bingham fluid. Again, with an increase in Debye-Hückel parameter (k), the EDL thickness decreases and this gives rise to flow non-uniformity within the thin EDL, resulting in the *plug flow radius* becoming widened. As a consequence the increase of *k* results in sharp declination in the velocity gradient. Although the advection coefficient function, -

K_1/Pe, clearly grows montonically with increment in Debye-Hückel parameter (k), the *gradient* of the profiles is reduced, in particular at larger values of *k*. Thus, the transport in micro-channel is clearly highly dependent on the EDL thickness. It is important to mention here that the influence of k, is more prominent at larger values of *k*, where the advection coefficient function profiles show larger differences. Larger *k* values indicate that the Debye length (which is a measure of the diffuse layer thickness and is dependent on the ionic concentration) is decreased.

7.3 Dispersion coefficient

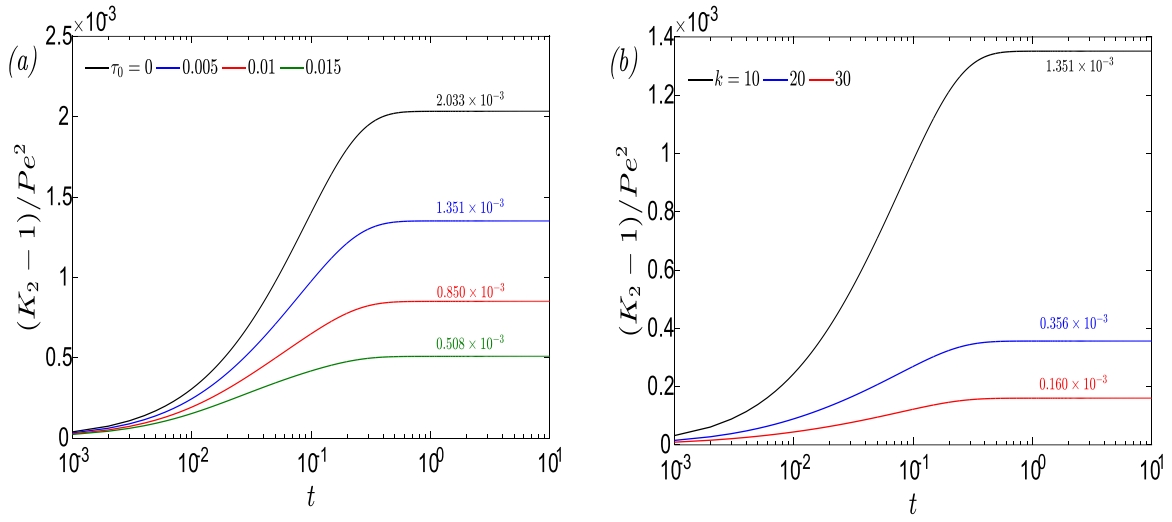

Figure 4: Dispersion coefficient for (a) various yield stress τ_0 with $k = 10$ (b) various values of Debye-Hückel parameter with $\tau_0 = 0.005$.

According to Taylor's dispersion analysis, the dispersion coefficient K_2 is relevant to studying the diffusion processes. In **Fig. 4**, the temporal variation of dispersion coefficient K_2 is investigated for variation in yield stress and Debye-Hückel parameter. As expected from Fig.4(a), the larger values of yield stress slow down the velocity in the axial direction and hence the radial diffusion is also minimized. Consequently, the value of the dispersion coefficient K_2 increases with time but decreases with greater yield stress. The profiles all ascend monotonically initially and after some time elapse the profiles assume plateau topologies in the steady state. A similar trend is computed in Fig. 4(b) where with increment in Debye-Hückel parameter (k) (i.e., decreasing EDL thickness), there is a decrement in dispersion coefficient function. This result is physically meaningful as the increase in k also results in a more uniform velocity distribution. Also, it must be noted that with the increment of τ_0 or k, dispersion coefficient reaches a stable value at a relatively small duration of time. **Figure 5** depicts the collective effects of τ_0 and k on K_2 at a fixed dimensionless time $t = 10$. It can be seen that with the increment of k (Fig 5a) the diffusion process becomes slow with respect to τ_0; though, although the

dispersion coefficient is not modified noticeably by k when τ_0 is small. In Fig. 5(b), dispersion coefficient with respect to k shows reducing in nature with the value of τ_0. A similar kind of result has been found in Paul and Ng [46] for $\tau_0 = 0$ (Newtonian fluid). It is notable that as k increases, the dispersion coefficient shows a sharp increment. After that, it shows a uniform decrement in nature and finally reaches a steady state. With lower values of k, the electro viscous effect is reduced, so a significant hike in dispersion coefficient is observed. Further, larger values of k leads to a more uniform velocity profile in across the microchannel, which reduces the radial diffusion and thereby decreases the effective dispersion coefficient.

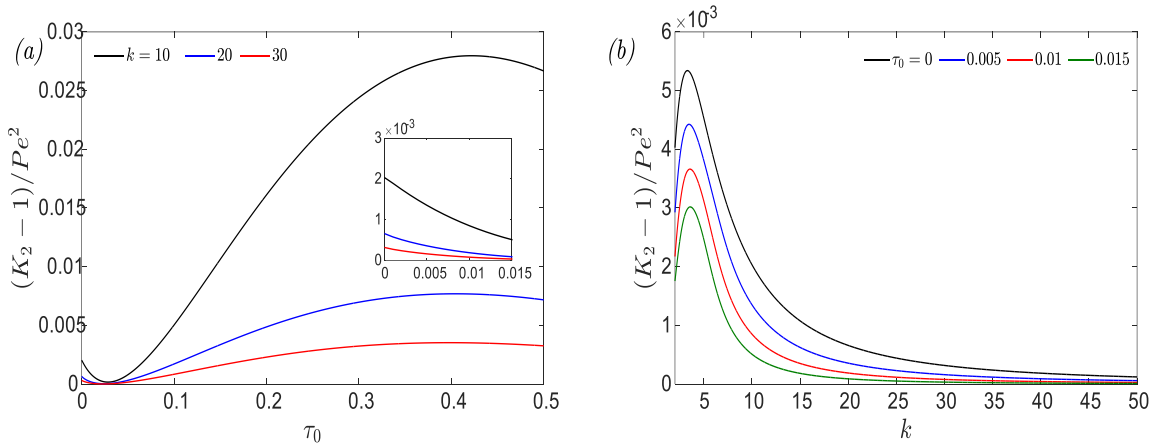

Figure 5: Variation of dispersion coefficient (K_2) at a fixed time t=10 (a) with yield stress and (b) Debye-Hückel parameter.

7.4 Apparent asymmetry coefficient

The apparent asymmetry coefficient (K_3) is the same as the *third-order statistical moment* (Wang and Chen [11]) for the present model without boundary wall reaction. Thus, the idea of K_3 can be used to describe the distribution of solute concentration. Fig.6 shows the effects of the yield stress (Bingham) and Debye-Hückel electro-osmotic parameters (τ_0 and k) on K_3 with time t. The trends are similar to that of the dispersion coefficient K_2 i.e. there is a *significant reduction* in the apparent asymmetry dispersion coefficient K_3 with increasing yield stress (τ_0) as observed in Fig. 6(a) and increasing Debye-Hückel parameter (k) as seen in Fig. 6(b). Both figures also demonstrate that the value of K_3 shows some increasing trend with time, although initially at small times the profiles are invariant. This may result in a positively skewed distribution, and the value of K_3 varies significantly at greater time values. Though, the nature of the apparent asymmetry coefficient is not ultimate (which is visualized in Fig.7). Further, in Figs. 6(a) and 6(b), we can see that K_3 becomes *uniform over large intervals of time*.

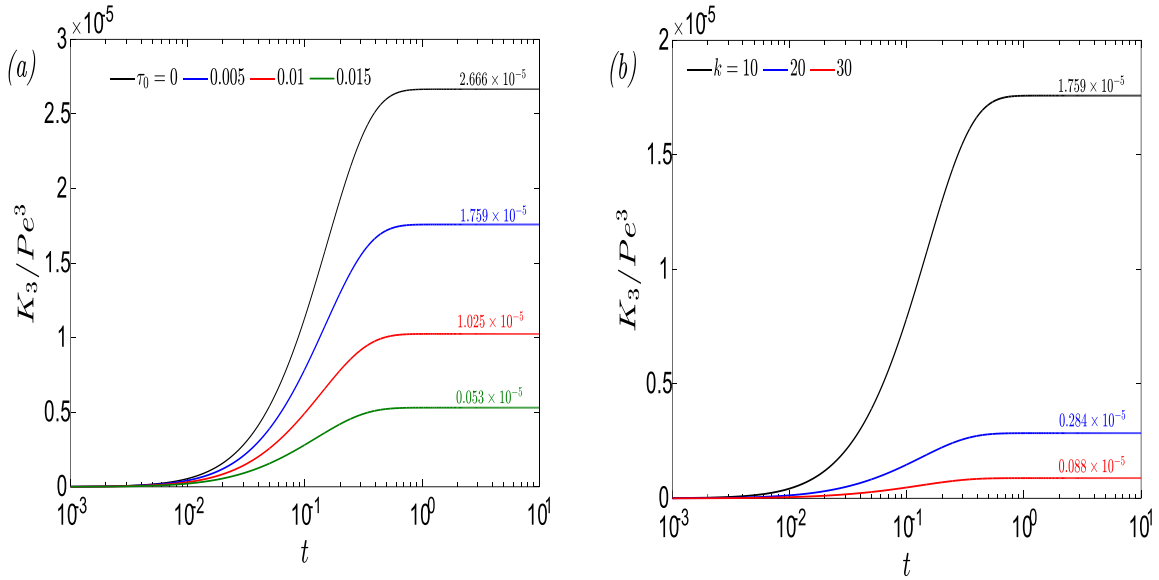

Figure 6: Apparent asymmetry coefficient K_3 for (a) various yield stress τ_0 with $k = 10$ (b) various value of Debye-Hückel parameter with $\tau_0 = 0.005$.

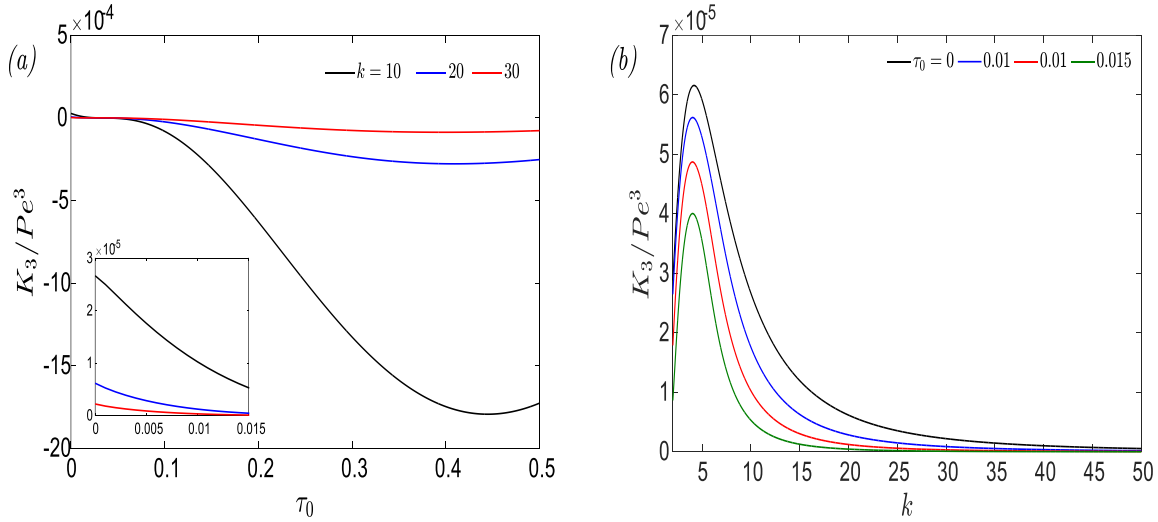

Figure 7: Transport coefficient K_3 at time $t = 10$ for (a) with yield stress and (b) Debye-Hückel parameter.

Figure 7 depicts the nature of the apparent asymmetry coefficient with respect to the influence of yield stress (τ_0) and the Debye-Hückel parameter (k) for a fixed dimensionless time $t = 10$. For small values of τ_0 we can see that K_3 decreases with k; however the contrary behaviour is observed for larger values of τ_0. The K_3 distribution is clearly modified by both τ_0 and k. As evident in Fig. 7(a), that the distribution becomes *negatively skewed* with τ_0 when $k = 10$. Similar patterns are computed for other values of k, however the impact is demonstrably reduced. Fig.7(b), depicts the variation of K_3 with respect to Debye-Hückel parameter (k) for some fixed values of yield stress (τ_0). The distribution curve is always *positively skewed* though the total area of the distribution curve is initially increasing with k, thereafter decreasing with k, and finally becomes stable with k. Via the inclusion of K_3 in the present model, it is therefore possible to *simultaneously address* the collective effects of both τ_0 and k

on K_3. Also, it must be noted that for sufficiently larger values of k, the asymmetric behaviour of the concentration distribution is independent of yield stress.

7.5 Mean concentration distribution

The axial distribution of mean concentration is shown in **Fig. 8** for fixed values of τ_0 and k considering different times, $t = 0.1, 0.5, 1$ and 5 , respectively. The trends qualitatively agree with previous works for Newtonian fluids [44]. Initially, the nature of the asymmetry is stronger in C_{mean} , however, after a certain time, the distribution assumes a Gaussian topology. Further, by Fig. 8 it is possible to discuss the importance of the third-order approximation of Gill's series expansion. In Fig. 8, the blue colored line is drawn for the second-order approximation of Gill's series expansion, and the black colored line corresponds to the third-order approximation. Clearly, at the initial times ($t = 0.1, 0.5$ and $t = 1$) the mean concentration is found to be negative for third-order approximation; which is not usual. Although this pattern may not always be obvious, however, it ensures that the truncation error reduces with third-order approximation. Meanwhile, for $t = 5$, this issue does not arise for second *or* third-order approximations.

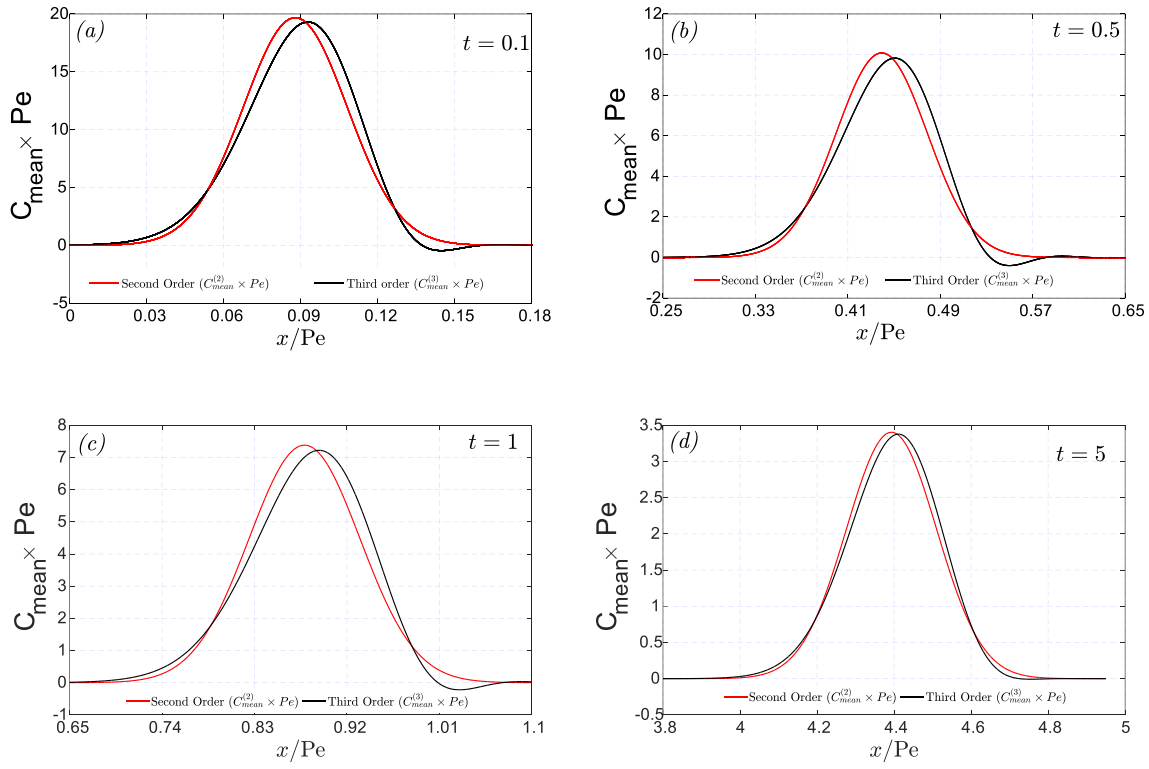

Figure 8: Mean concentration distribution at different time instances with for fixed yield stress ($\tau_0 = 0.005$) and Debye-Hückel parameter ($k = 10$).

Hence, the large time behaviour of the mean concentration distribution can be studied by second-order approximation. However, the use of third or higher orders of approximation in Gill's series expansion is justified for examining the *small and moderate time behavior* of transport coefficients.

Finally, in Fig.9, the mean concentration distribution in the axial direction is studied for various values of yield stress and Debye-Hückel parameter when $t = 10$. Increase in yield stress increases the height of C_{mean} (Fig.9(a)) and has been reported earlier [36]. As the yield stress increases, the solute spreading process is more significantly affected by flow resistance, and thus peak height (amplitude) of mean concentration increases. Fig. 9(b) also shows that with increasing *k* values, the peaks of the mean concentration are strongly enhanced. However the peaks are displaced *to the left* corresponding to lower values of the abscissa (*x/Pe*) with increment in Bingham yield stress (τ_0) whereas they are displaced *to the right* corresponding to higher values of the abscissa (*x/Pe*) with increment in Debye-Hückel parameter (*k*). *Therefore while both non-Newtonian yield stress and electro-osmotic effects boost the* mean concentration heights, they *modify the distribution of these peaks* in a different fashion.

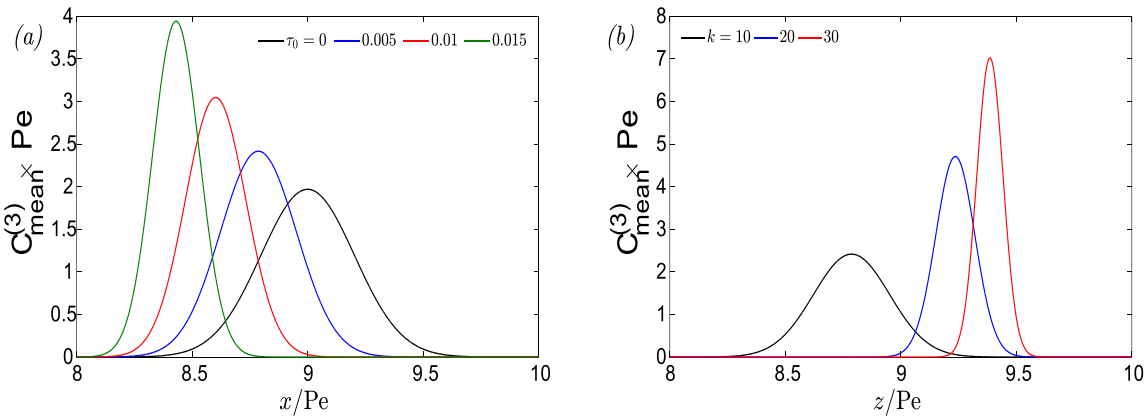

Figure 9: Second order mean concentration distribution at time t=10 (a) various yield stress τ_0 with $k = 10$ (b) various value of Debye-Hückel parameter with $\tau_0 = 0.005$.

8.Conclusions

In the present work, a mathematical study has been presented to investigate the *transport of a neutral solute in electro-osmotic flow of an ionic Bingham plastic fluid through a micro-channel bounded by two parallel-plates*. Gill's generalised dispersion model, which considers up to third-order approximation, has been deployed to quantify the transport mechanism by means of three coefficients- *the advection coefficient, dispersion coefficient, and apparent asymmetry coefficient*, respectively. Further, the mean concentration distribution is also analyzed considering these transport coefficients. The present work constitutes a novel analysis motivated by emerging applications in bio-microfluidics

and electro-osmotic micro-mixers. The important findings from this study may be summarized as follows:

- The average flow velocity (equivalent to the advection coefficient) is reduced with an increment in Bingham yield stress and Debye-Hückel parameter.

- The magnitude of the dispersion coefficient K_2 diminishes with time as the values of yield stress and the Debye-Hückel parameter increase. If the yield stress value is very small, the Debye-Hückel parameter has no significant effect on the dispersion coefficient for a given time. The results are comparable to that of a Newtonian fluid model when the yield stress is zero.

- The apparent asymmetry coefficient K_3 clearly shows that the *nature of asymmetry* is strongly dependent on both yield stress and Debye-Hückel parameter ranges. There is a significant depletion in the apparent asymmetry dispersion coefficient K_3 with increasing yield stress (τ_0) and increasing Debye-Hückel parameter (k). However for a very thin EDL thickness the type of distribution is *independent of yield stress*.

- The mean concentration distribution appears asymmetric at smaller times, and thereafter evolves into a Gaussian profile.

- As the yield stress increases, the solute spreading process is more substantially impacted by flow resistance (viscous effects), and thus peak height (amplitude) of mean concentration increases.

- With a second-order approximation in Gill's series expansion, one can study the asymptotic behaviour of the dispersion process *at large times*. However, to scrutinize behaviour *at small and moderate times*, a third or higher order approximation is required in Gill's series expansion.

The current study has considered a simple non-Newtonian model i.e. Bingham fluid. Future investigations in electro-osmotic hydrodynamic dispersion may explore more elegant rheological models e.g. Eringen's micropolar model, and efforts in this direction are currently underway.

Acknowledgements

We express our sincere thanks to the Reviewer for his/her critical review and comments on the manuscript. These comments have helped to improve the clarity of the article.

References

[1] G. I. Taylor, *Proceedings of the Royal Society A: Mathematical, Physical and Engineering Sciences* **1953** *219*(1137), 186.

[2] R. Aris, *Proceedings of the Royal Society A: Mathematical, Physical and Engineering Sciences* **1956** *235*(1200), 67.

[3] W. N. Gill, *Proceedings of the Royal Society A: Mathematical, Physical and Engineering Sciences* **1967**, *298* (1454), 335.

[4] P. C. Chatwin, *Journal of Fluid Mechanics* **1970**, *43*(2), 321.

[5] W. N. Gill, R Sankarasubramanian, *Proceedings of the Royal Society A: Mathematical, Physical and Engineering Sciences* **1970**, *316*(1526), 341.

[6] N. G. Barton, *Journal of Fluid Mechanics* **1983**, *126*, 205.

[7] B. S. Mazumder, Samir K Das, *Journal of Fluid Mechanics* **1992**, 239, 523.

[8] Chiu-On Ng, *Proceedings of the Royal Society A: Mathematical, Physical and Engineering Sciences* **2006** *462*(2066), 481.

[9] Zi Wu, G. Q. Chen, *Journal of Fluid Mechanics* **2014**, *740*, 196.

[10] Jyotirmoy Rana, P. V. S. N. Murthy, *Journal of Fluid Mechanics* **2016**, *793*, 877.

[11] Ping Wang, G. Q. Chen, *International Journal of Heat and Mass Transfer* **2016**, *95*, 131.

[12] Ashis Kumar Roy, Apu Kumar Saha, Sudip Debnath, *International Communications in Heat and Mass Transfer* **2020**,*110*,104369.

[13] Sudip Debnath, Weiquan Jiang, Mingyang Guan, Guoqian Chen, *Physics of Fluids **2022**, 34*(2), 027106.

[14] B Wunderlich, D Nettels, B Schuler, *Lab on a Chip* **2014**, *14*(1), 219.

[15] Jiafeng Yao, Tatsuya Kodera, Hiromichi Obara, Michiko Sugawara, Masahiro Takei, *Biomicrofluidics* **2015**, *9*(4), 044129.

[16] K Hockemeyer, C Janetopoulos, A Terekhov, W Hofmeister, A Vilgelm, Lino Costa, JP Wikswo, A Richmond, *Biomicrofluidics* **2014**, *8*(4), 044105.

[17] Zhigang Wu, Nam-Trung Nguyen, Xiaoyang Huang, *Journal of Micromechanics and Microengineering* **2004**, *14*(4), 604.

[18] Amal Ibrahim, Rémi Meyrueix, Gauthier Pouliquen, You Ping Chan, Hervé Cottet, *Analytical and bioanalytical chemistry* **2013,** *405*(16), 5369.

[19] Cecilia IAV Santos, Miguel A Esteso, Victor MM Lobo, Ana MTDPV Cabral, Ana CF Ribeiro, *The Journal of Chemical Thermodynamics* **2015**, *84*, 76.

[20] Douglas E Smith, Thomas T Perkins, Steven Chu, *Macromolecules* **1996**, *29*(4), 1372.

[21] ET Lagally, I Medintz, RA Mathies, *Analytical chemistry* **2001**, *73*(3), 565.

[22] Yang Huiqian, Nam-Trung Nguyen, Xiaoyang Huang, in *Journal of Physics: Conference Series, IOP Publishing, **2006**, p. 023*.

[23] Chee G Koh, Woei Tan, Ming-qi Zhao, Antonio J Ricco, Z Hugh Fan, *Analytical Chemistry* **2003**, *75*(17), 4591.

[24] Eric T Lagally, Peter C Simpson, Richard A Mathies, *Sensors and Actuators B: Chemical* **2000**, *63*(3), 138.

[25] Vahid Hoshyargar, Atieh Khorami, Seyed Nezameddin Ashrafizadeh, Arman Sadeghi, *Sensors and Actuators B: Chemical* **2018**, *255*, 3585.

[26] Morteza Dejam, *International Journal of Heat and Mass Transfer* **2019**, *136*, 87.

[27] Fengqin Li, Yongjun Jian, *International Journal of Heat and Mass Transfer* **2019**, *141*, 1066.

[28] Reza Talebi, Seyed Nezameddin Ashrafizadeh, Arman Sadeghi, *Chemical Engineering Science* **2021**, *229*, 116058.

[29] Jacob H Masliyah, Subir Bhattacharjee, Electrokinetic and colloid transport phenomena, *John Wiley & Sons*, **2006**.

[30] M Keith Sharp, *Annals of Biomedical Engineering* **1993**, *2l*(4), 407.

[31] R. K. Dash, G Jayaraman, K. N. Mehta, *Annals of Biomedical Engineering* **2000**, *28*(4), 373.

[32] Jyotirmoy Rana, P. V. S. N. Murthy, *Proceedings of the Royal Society A: Mathematical, Physical and Engineering Sciences* **2016**, *472*(2193), 20160294.

[33] Jyotirmoy Rana, P. V. S. N. Murthy, *Proceedings of the Royal Society A: Mathematical, Physical and Engineering Sciences* **2017**, *473*(2204), 20170427.

[34] Sudip Debnath, Apu Kumar Saha, B. S. Mazumder, Ashis Kumar Roy, *Chinese Journal of Chemical Engineering* **2017**, *25*(7), 862.

[35] [35] Sudip Debnath, Apu Kumar Saha, B. S. Mazumder, Ashis Kumar Roy, Physics of Fluids 2017 29(9), 097107.

[36] Ashis Kumar Roy, O. Anwar Bég, *International Communications in Heat and Mass Transfer* **2021**, *122*, 105169.

[37] Ashis Kumar Roy, Apu Kumar Saha, Sudip Debnath, *Periodica Polytechnica Chemical Engineering* **2018**, *62*(2), 215.

[38] JC Arcos, F Méndez, EG Bautista, O Bautista, *Journal of Fluid Mechanics* **2018**, *839*, 348.

[39] Siddhartha Mukherjee, Jayabrata Dhar, Sunando DasGupta, Suman Chakraborty, *Proceedings of the Royal Society A: Mathematical, Physical and Engineering Sciences* **2019**, *475*(2221), 20180522.

[40] Chien-Hsuan Ko, Di Li, Amirreza Malekanfard, Yao-Nan Wang, Lung-Ming Fu, Xiangchun Xuan, *Electrophoresis* **2019**, *40*(10), 1387.

[41] Hsin-Yu Wu, Cheng-Hsien Liu, *Sensors and Actuators A: Physical* **2005**, *118*(1), 107.

[42] Cunlu Zhao, Chun Yang, *Advances in colloid and interface science* **2013**, *201*, 94.

[43] Du-Soon Choi, Sungchan Yun, WooSeok Choi, *Micromachines* **2018**, *9*(10), 504.

[44] Wei-Quan Jiang, Ping Wang, G. Q. Chen, *Journal of Hydrology* **2017**, *549*, 340.

[45] W. Q. Jiang, G. Q. Chen, *International Journal of Heat and Mass Transfer* **2018**, *127*, 34.

[46] Suvadip Paul, Chiu-On Ng, *Acta Mech. Sin.* **2012**, *28*(3), 631.

[47] Stewart K Griffiths, Robert H Nilson, *Analytical Chemistry* **1999**, *71*(24), 5522.

[48] Sudip Debnath, Apu Kumar Saha, B. S. Mazumder, Ashis Kumar Roy, *Journal of Engineering Mathematics* **2019**, 116(1), 1.

[49] Ashis Kumar Roy, Apu Kumar Saha, R Ponalagusamy, Sudip Debnath, *Korea-Australia Rheology Journal* **2020**, *32*(4), 287.

[50] G Mohiuddin Mala, Dongqing Li, J. D. Dale, *International Journal Heat Mass Transfer* **1997**, *40*(13), 3079.

****